Science Advances
AAAS

advances.sciencemag.org/cgi/content/full/6/48/eabc8733/DC1

Supplementary Materials for

Visualization nanozyme based on tumor microenvironment "unlocking" for intensive combination therapy of breast cancer

Zhiyi Wang, Ziyuan Li, Zhaoli Sun, Shuren Wang, Zeeshan Ali, Sihao Zhu, Sha Liu, Qiushi Ren, Fugeng Sheng, Baodui Wang, Yanglong Hou*

*Corresponding author. Email: hou@pku.edu.cn

Published 27 November 2020, *Sci. Adv.* **6**, eabc8733 (2020)
DOI: 10.1126/sciadv.abc8733

The PDF file includes:

Other Supplementary Material for this manuscript includes the following:

(available at advances.sciencemag.org/cgi/content/full/6/48/eabc8733/DC1)

Materials. Ammonium bromide (NH4Br, 99%) and terephthalic acid (99.9%) were purchased from J&K Chemicals. Oleylamine (OAm, tech. 70 %), oleic acid (OA, 99%), Octadecylamine (ODA, 90%), 1-Octadecene (ODE; 90%), 1-Dodecanethiol (DT, 98%), $AgNO_3$, $(C_2H_5)2NCS_2Na_3{\cdot}H_2O$ [Na(DDTC)], DSPE-PEG-NH_2 (MW=5000 Da, 98%), DSPE-PEG-NHS (MW=5000 Da, 95%), calcein-AM and propidium iodide (PI) were purchased from Sigma Aldrich. Iron pentacarbonyl were from Tianyi Co. Ltd, Jiangsu, China. Dihydrorhodamine 123 (DHR123) was purchased from Thermo Fishcer Scientific (Waltham, MA, USA). iRGD peptide [c(CRGDKGPDC), 98.62%] was purchased from MedChemExpress. Murine Bevacizumab was purchased from eBioscience in USA. All the chemicals were used without additional purification, except $CHCl_3$, triethylamine, and were performed under argon utilizing a homemade heating apparatus, four-neck bottles (Synthware), a glove box (MIKROUNA) and Ar/N_2/vacuum lines. All the dialysis bags (Mr = 8000~14000) were obtained from Shanghai Med. These NPs were synthesized by using standard air-free procedures.

Instruments. The microstructure of the prepared materials was investigated by transmission electron microscopy (TEM, HT-7700, FEI Tecnai T20 and FEI Tecnai F30). HRTEM was carried out on a FEI Tecnai F30 microscope (300kV). Reinforced carbon membrane support grid was used to obtain the EDS mapping. XPS measurements were performed on an imaging X-ray photoelectron spectrometer using Al Kα radiation (Axis Ultra DLD, Kratos Analytical Ltd.). All the collected spectra were calibrated with contaminated C 1s peak at 284.8eV, and were analyzed using CasaXPS software (2.3.12 Dev7). X-ray diffraction (XRD) patterns were measured on a Rigaku SmartLab 9 kW X-ray powder diffractometer with Cu-Ka radiation at 45 kV and 200 mA. Nicolet FTIR spectrometer (Magna-IR 750) was used for FTIR measurements. Physical property measurement system (PPMS-9, Quantum Design, USA) was used to measure the magnetization. Multi-dimensional confocal microfluorescence imaging system (FLIM+confocal+AFM, Q2, ISS-USA) was used for fluorescence imaging in NIR-II at cell level. Fluorescence imaging system in NIR-II for small animals in vivo is self-assembled. Inductively coupled plasma-atomic emission spectrometer (ICP-AES, Prodigy 7, and Leeman, USA) was used to quantify the concentrations of Fe. Dynamic light scattering (DLS) was measured using a particle size analyzer (Zetasizer Nano ZS90, Malvern, England). UV 1750 spectrophotometer (Shimadzu, Japan) was used to measure the UV-vis absorbance. Infrared thermal imaging instrument (FLIR A325SC camera) was used to record the temperature detection and thermal image; 808nm high-power multimode pump laser (Shanghai Connect iber Optics Co.) was used for NIR laser.

Preparation of Ag (DDTC). In a typical synthetic process, 0.05 mol of $AgNO_3$ and $(C_2H_5)_2NCS_2Na_3{\cdot}H_2O$ were firstly dissolved in 100 ml of distilled water, respectively. Then, the two solutions were mixed with stirring in a 500 ml beaker. After constant ambient condition for 3 h, the resulting yellow precipitate was filtered, washed with distilled water, and dried in air at 60 °C.

Synthesis of monodisperse Ag_2S QDs. Ag_2S QDs were synthesized according to previous reports *(25,41)*. A typical procedure is described as follows: a mixture of 0.1 mmol of $(C_2H_5)_2NCS_2Ag$ and 10 g of DT was added into a three-necked flask. After oxygen was removed from the flask, the solution was heated to 210 ℃ and kept at this temperature for 1 h under N_2 atmosphere. When the mixture was cooled to room temperature, excess of ethanol was added, and then the precipitates were collected through centrifugation, and redispersed into hexane.

Synthesis of DSPE-PEG-iRGD. DSPE-PEG-iRGD was synthesized by the amidation between DSPE-PEG-NHS and tumor-homing penetration peptide iRGD (CRGDKGPDC). DSPE-PEG-NHS (100.0 mg, 0.02 mmol) and iRGD

(CRGDKGPDC) (18.96 mg, 0.02 mmol) were dissolved in 10 mL of HEPES buffer (pH=7.2). Subsequently, the reaction mixture was stirred for 12 h at 4 ℃. Finally, the reaction product was isolated and purified by recrystallization.

Photothermal effect and photostability of Ag_2S@Fe_2C-DSPE-PEG. A total of 350 μL of Ag_2S@Fe2C-DSPE-PEG dispersions in a 96-well cell culture plate with different concentrations (0, 10, 20, 30 and 40 mg L-1) were irradiated with a laser (808 nm, 0.3 W cm-2) for 5 min, and their temperature in solution was recorded by an online type thermocouple thermometer. Similarly, in order to study the influence of optical density on photothermal conversion, 350 μL of 20 mg L-1 Ag_2S@Fe_2C-DSPE-PEG dispersions was irradiated with an 808 nm laser with different power density (0.1, 0.2, 0.3, 0.4 and 0.5 W cm-2) for 5 min. The change of temperature in solution was recorded. The photostability of Ag_2S@Fe_2C-DSPE-PEG dispersions (60 mg L-1) was estimated by irradiating in a quartz cuvette with a laser (808 nm, 0.3 W cm-2) for 5 min, and then cooling to room temperature without irradiation. The photostability was test by repeating such processes three times.

Cell culture. NIH3T3, and 4T1 cell lines were obtained from the Cancer Institute and Hospital of the Chinese Academy of Medical Science. All cell-culture-related reagents were purchased from Invitrogen. RPMI-1640 culture medium supplemented with 10% FBS and 1% penicillin/streptomycin was used to culture cells at 37 °C under 5% CO2 with 100% humidity.

Cytotoxicity by CCK-8 assay. NIH3T3 or 4T1 cells (1×104 cells per well) seeded into a 96-well cell culture plate were incubated with Ag_2S@Fe_2C-DSPE-PEG in different Fe concentrations (0, 2, 4, 8, 12, 16 and 20 mg L^{-1}) for 48 h at 37 °C under 5% CO2. The relative cell viabilities were determined by a standard CCK-8 viability assay. The absorbance of each well was measured with a luminescence microplate reader (Bio-Rad 680) at 450nm.

Bio-TEM characterization. Bio-TEM was utilized to determine the subcellular distribution of the Ag_2S@Fe_2C-DSPE-PEG-iRGD in treated 4T1 cells. 4T1 cells were seeded in a 35 mm culture dishes (10^5 cells in each well). The cells were then incubated with Ag_2S@Fe_2C-DSPE-PEG-iRGD for 12 h. Then cells were irritated with laser for 5 min (808 nm, 0.3 W cm^{-2}), and then incubated 4 h before fixing. The cells were washed three times by PBS, fixed using paraformaldehyde and osmium tetraoxide, and then dehydrated with ethanol. The cells were embedded in Spurr resin, sectioned to 70 nm in thickness. After that the section observed under TEM.

Animals and tumor model. All experiments involving animals were performed in accordance with the guidelines of the Institutional Animal Care and Use Committee (IACUC) of Peking University, Beijing, China. Balb/c nude mice with four to five-week-old and the average weight of 20 g were provided by the Beijing Center for Disease Control and Prevention, Beijing, China. SPF animal house was provided to mice under a 12 h light and 12 h darkness cycle and were fed a standard laboratory diet and tap water ad libitum. 4T1 cells (0.2 mL cells in 1640 culture medium without FBS) were injected to mice with subcutaneously at the right axillary region.

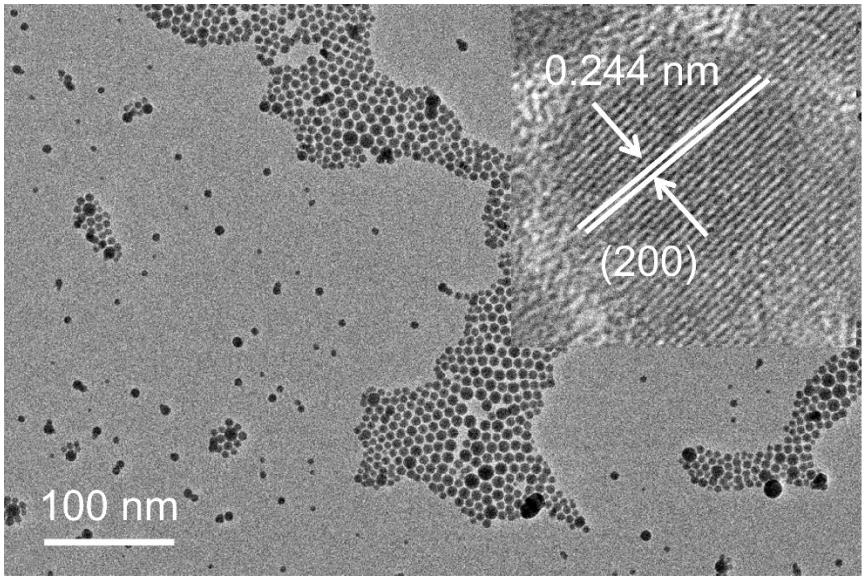

Fig. S1. TEM image of Ag_2S QDs.

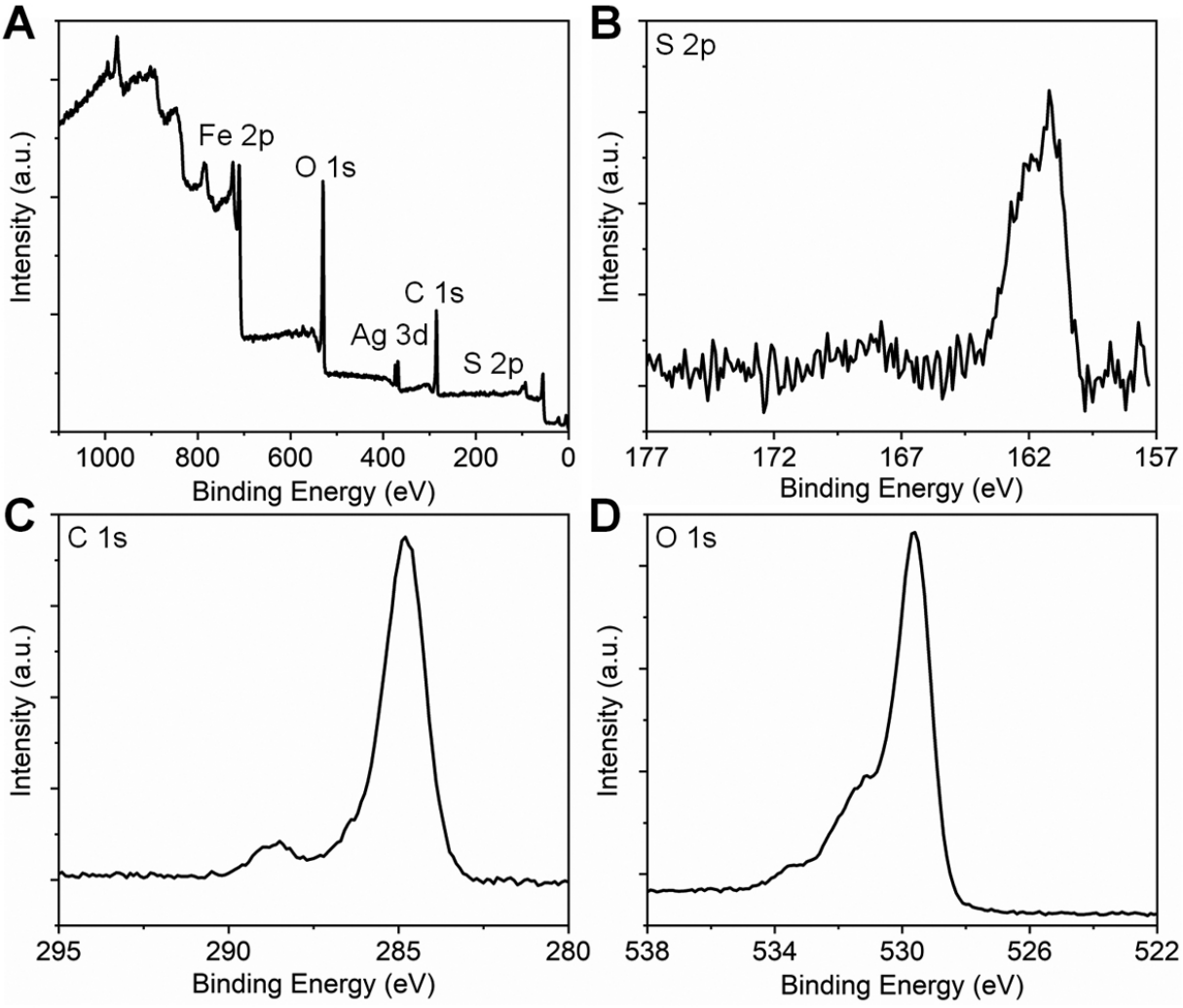

Fig. S2. XPS of Ag_2S@Fe_2C NPs. (A) and High resolution XPS of (B) S 2p, (C) C 1s and (D) O 1s.

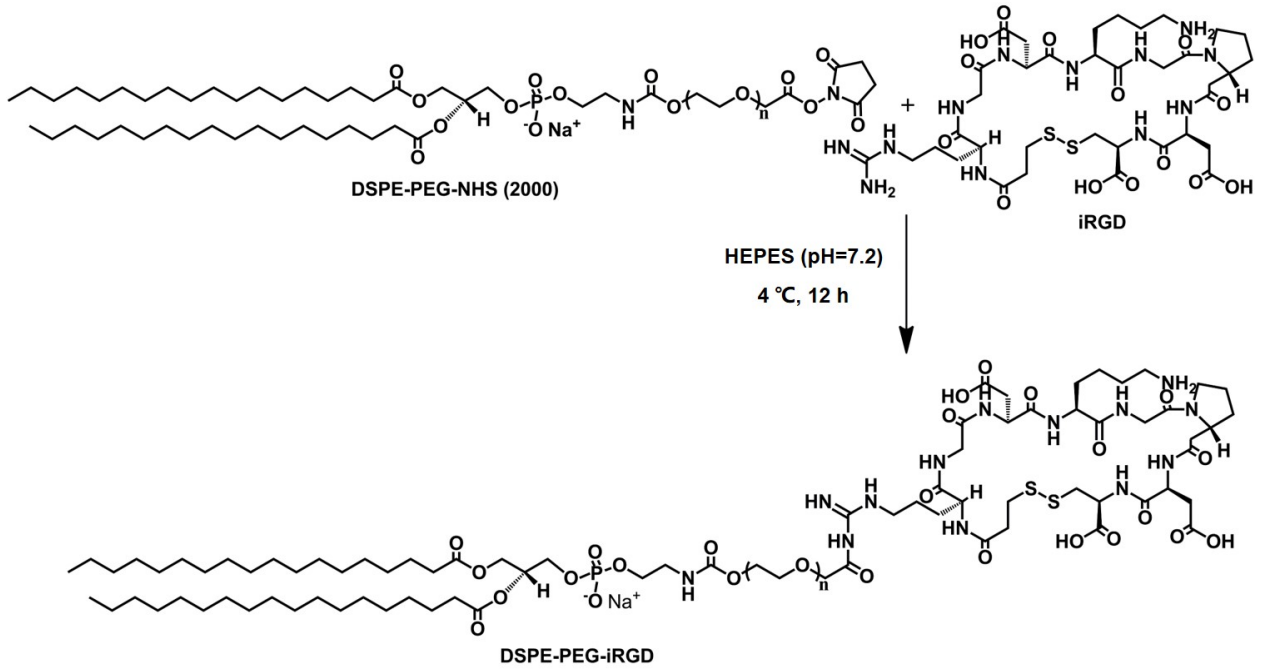

Fig. S3. Synthetic route of the DSPE-PEG-iRGD.

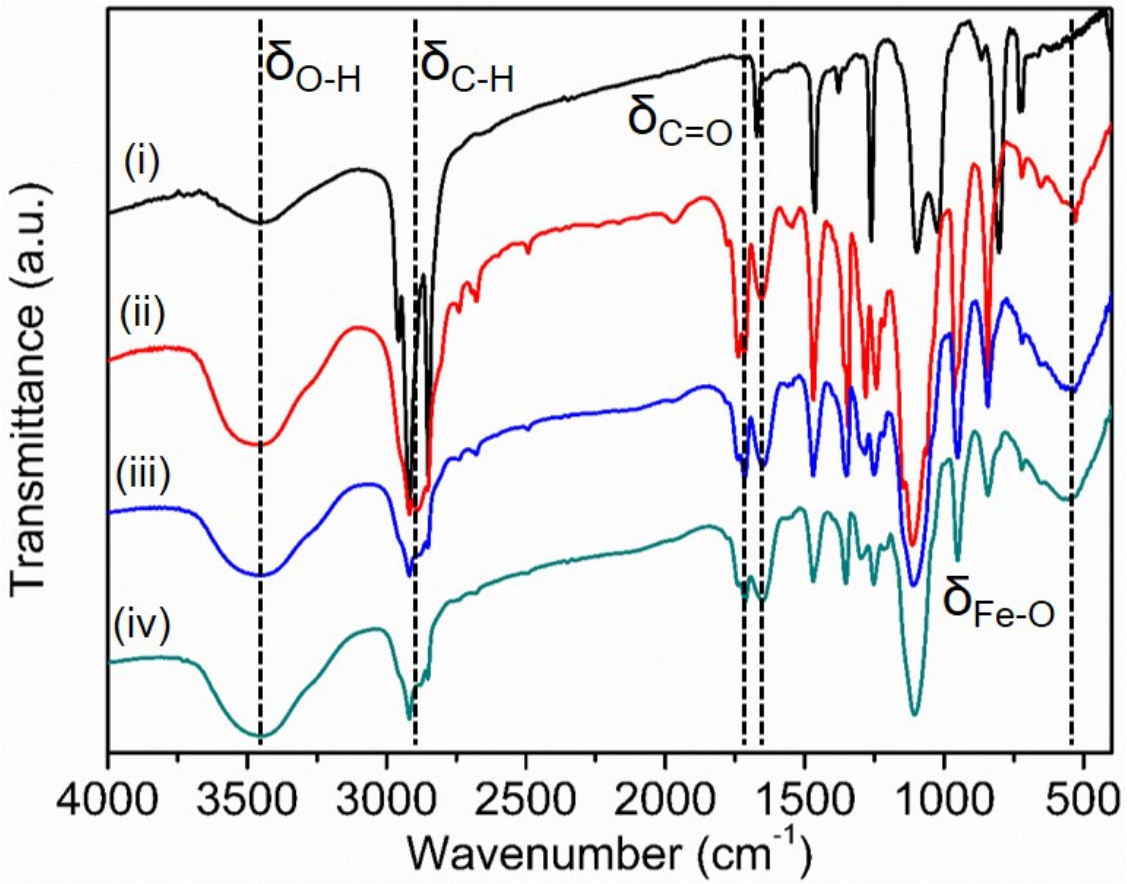

Fig. S4. FTIR characterization. i: DSPE-PEG-NHS, ii: $Ag_2S@Fe_2C$, iii: $Ag_2S@Fe_2C$- DSPE-PEG, iv: $Ag_2S@Fe_2C$-DSPE-PEG-iRGD.

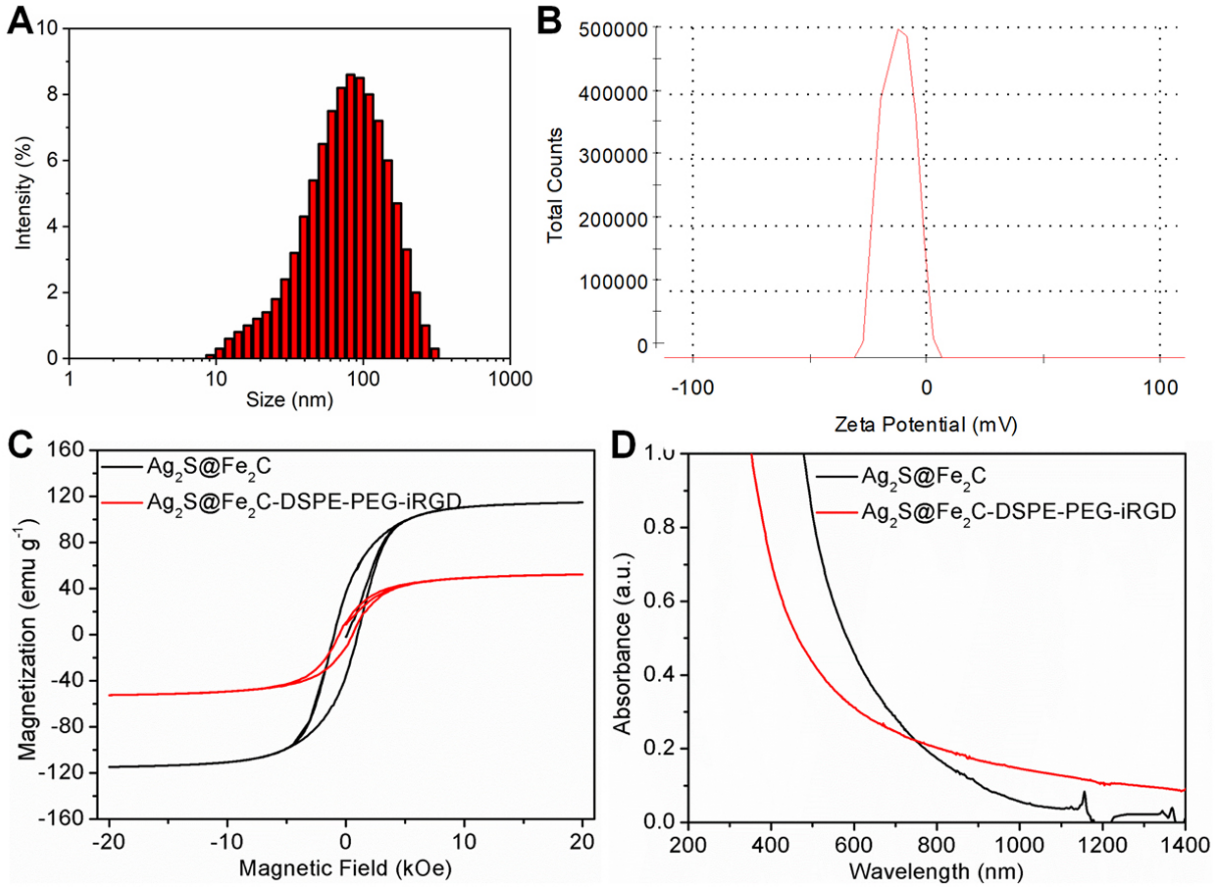

Fig. S5. Characterization of the as-synthesized Ag_2S@Fe_2C-DSPE-PEG-iRGD. (A) Hydrodynamic diameters measured by DLS for the Ag_2S@Fe_2C-DSPE-PEG-iRGD (90.1±20.3 nm, PDI=0.555). (B) The zeta potential distribution of Ag_2S@Fe_2C-DSPE-PEG-iRGD (-12.2 mV). (C) Magnetic hysteresis loops of the Ag_2S@Fe_2C and Ag_2S@Fe_2C-DSPE-PEG-iRGD at 298 K. (D) UV-vis absorbance spectra of Ag_2S@Fe_2C-DSPE-PEG-iRGD.

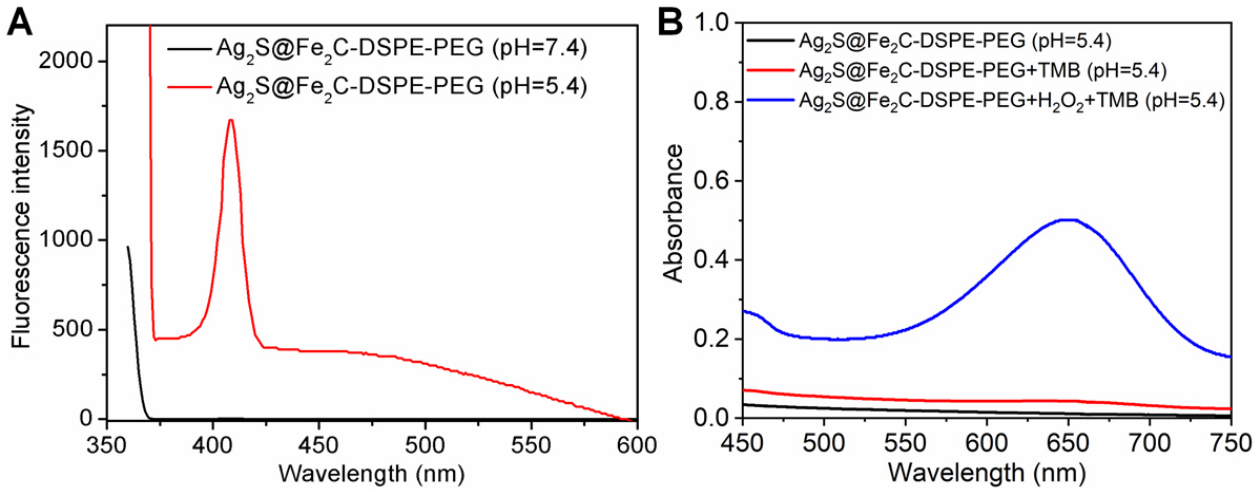

Fig. S6. *In vitro* performance evaluation of nanozyme. (A) Fluorescence spectrum of Ag_2S@Fe_2C-DSPE-PEG dispersed in pH value of 7.4 and 5.4 PBS buffer solution after 7 days. (B) Comparison of peroxidase-like activity for Ag_2S@Fe_2C-DSPE-PEG under different catalytic substrates in PBS (pH=5.4).

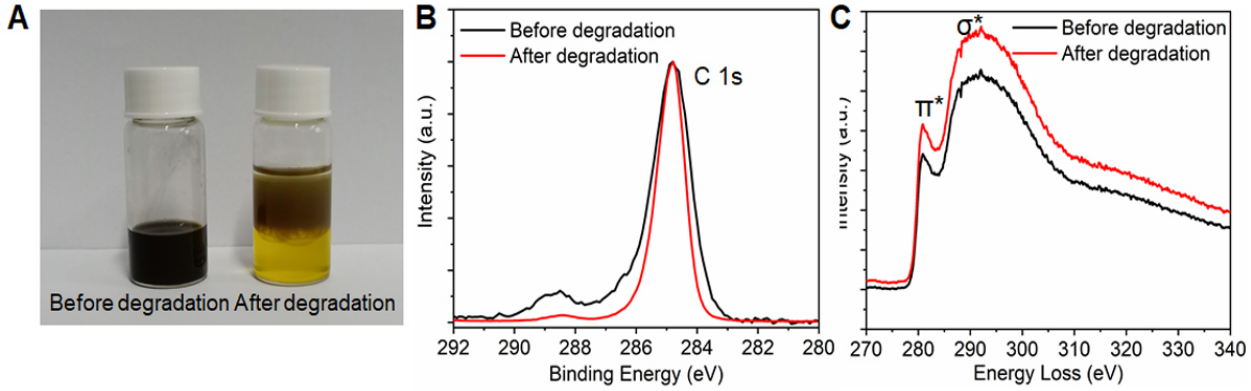

Fig. S7. Characterization of Ag_2S@Fe_2C before and after degradation in acidic system. (A) Photographs of obtained from Ag_2S@Fe_2C before and after degradation in HCl solution (1 mol L^{-1}) in 12 h. (Photo credit: Zhiyi Wang, Peking University, China.) (B) Normalized high-resolution XPS spectra of C 1s obtained from Ag_2S@Fe_2C before and after degradation in HCl solution (1 mol L^{-1}). (C) Carbon K-edge electron energy loss spectra of obtained Ag_2S@Fe_2C before and after degradation in HCl solution (1 mol L^{-1}).

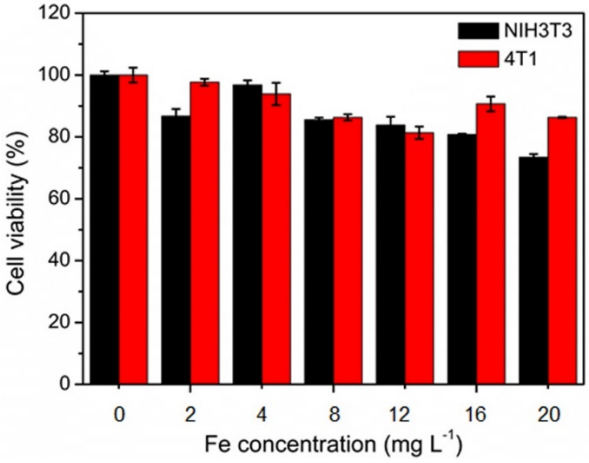

Fig. S8. Cytotoxicity evaluation of Ag_2S@Fe_2C-DSPE-PEG-iRGD in 4T1 and NIH3T3 cells for 24 h. (Error bars, mean±SD, n=6).

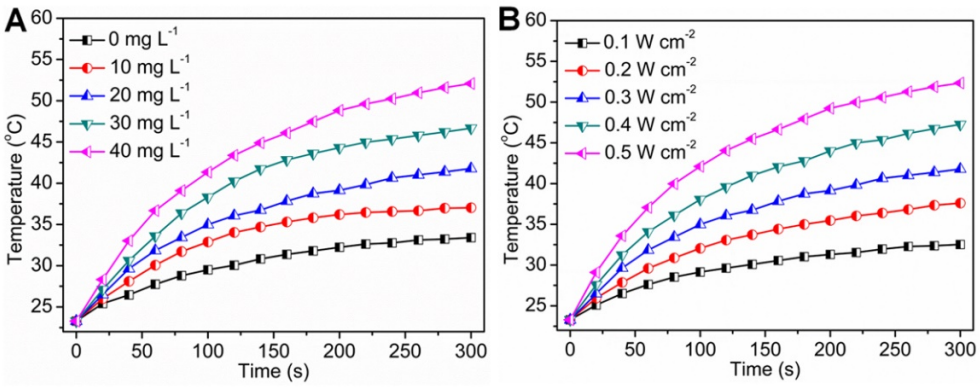

Fig. S9. The condition optimization of the experiment of photothermal conversion *in vitro*. (A) Temperature curves of Ag_2S@Fe_2C-DSPE-PEG-iRGD dispersions with concentrations of 0, 10, 20, 30 and 40 mg L^{-1} under 808 nm irradiation at a laser power density of 0.3 W cm^{-2} in 5 min. (B) Temperature curves of Ag_2S@Fe_2C-DSPE-PEG-iRGD dispersions with different power densities (0.1, 0.2, 0.3, 0.4, and 0.5 W cm^{-2}) with the concentration of 20 mg L-1 under 808 nm laser irradiation in 5 min.

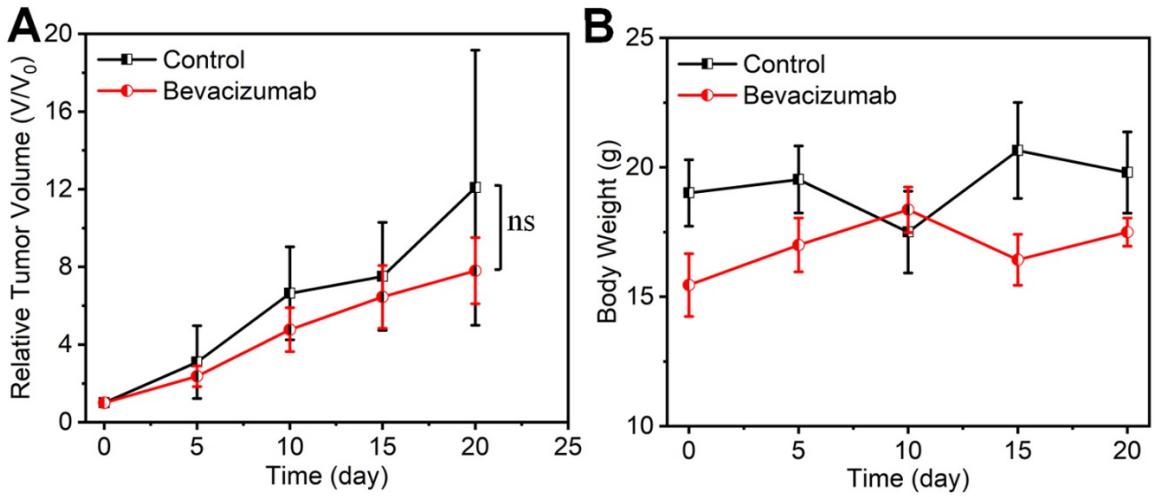

Fig. S10. Therapeutic effect of bevacizumab. (A) Volume change of tumor after intraperitoneal injection of saline and bevacizumab. (B) Body weight change of mice after injection of saline and bevacizumab (Error bars, mean±SD, n=5, unpaired t test).

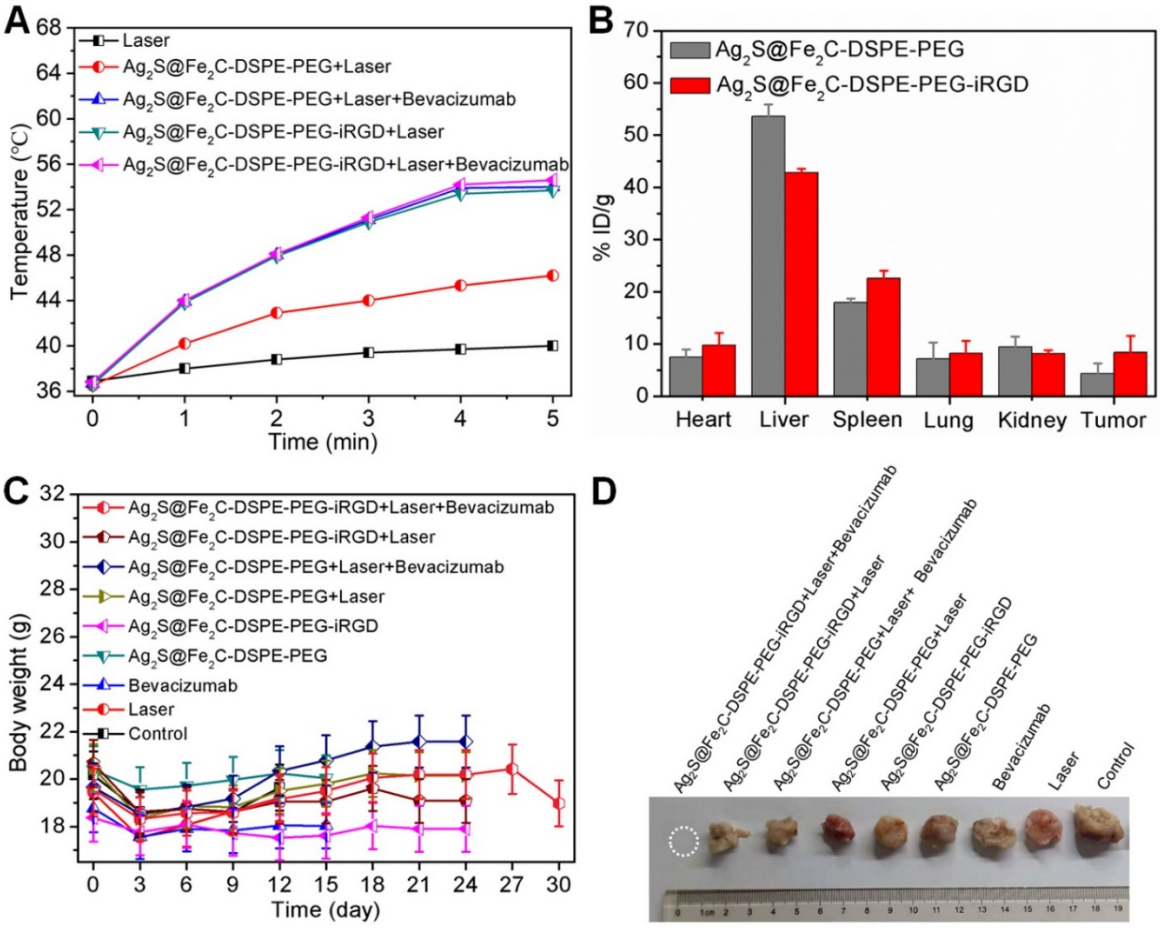

Fig. S11. Therapeutic effect in vivo. (A) Temperature change curves of 4T1 tumor-bearing mice at different time points in the different treatment groups (Laser: 808 nm, 0.3 W cm^{-2}). (B) The biodistribution of Ag_2S@Fe_2C-DSPE-PEG and Ag_2S@Fe_2C-DSPE-PEG-iRGD with same concentration after *i.v.* injection for 3 days by ICP-MS. (C) Body weight change of mice in the different treatment (five mice per group). (D) Photographs of the excised tumors in different treatment group after 30 days. (Photo credit: Zhiyi Wang, Peking University, China.) Error bars, mean±SD, n=5.

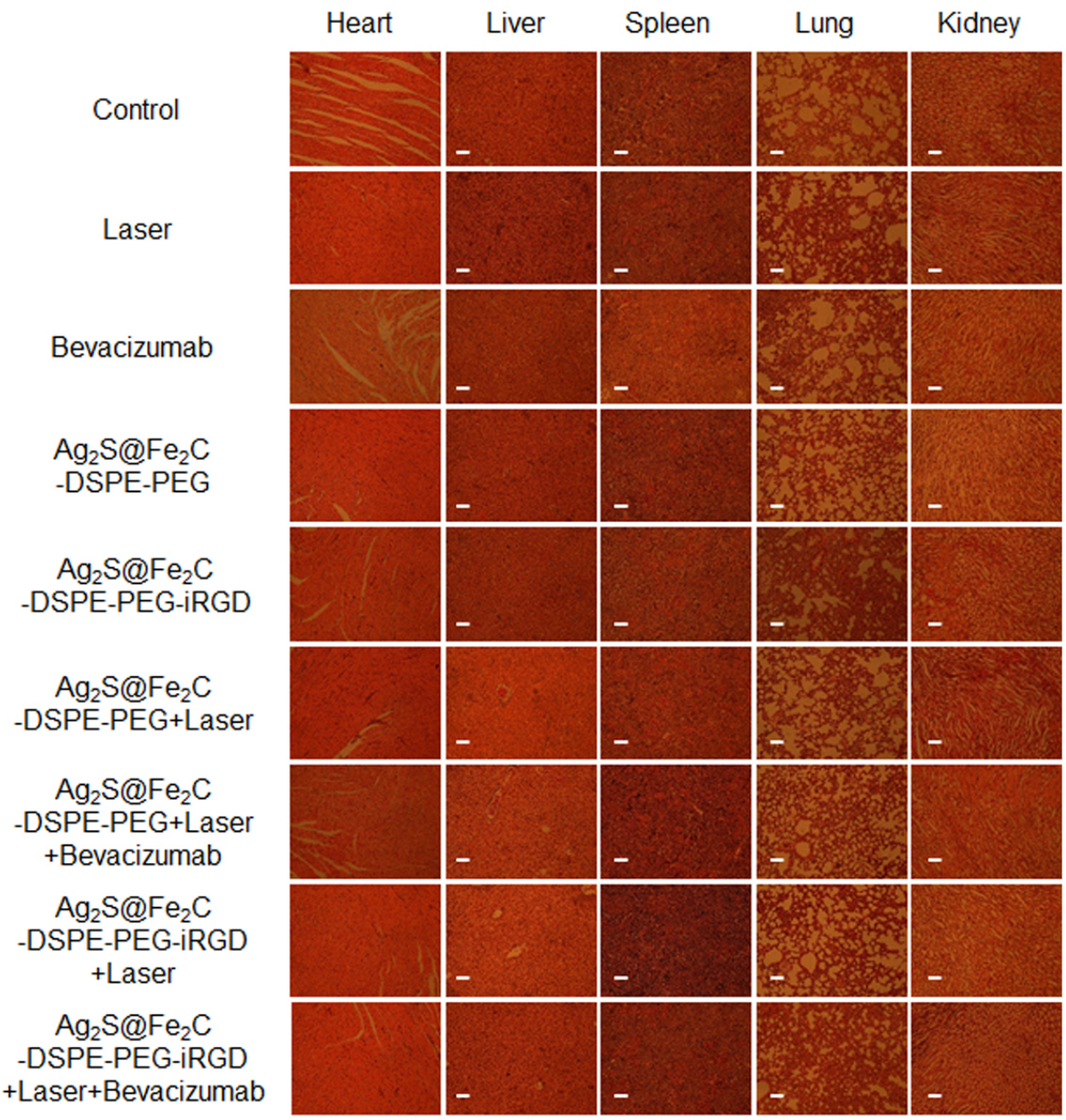

Fig. S12. H&E stained images of major organs collected from different groups of mice. (major organs: heart, kidney, liver, lung and spleen, Bars are 50 μm)

REFERENCES AND NOTES

1. N. Harbeck, F. Penault-Llorca, J. Cortes, M. Gnant, N. Houssami, P. Poortmans, K. Ruddy, J. Tsang, F. Cardoso, Breast cancer. *Nat. Rev. Dis. Primers.* **5**, 66 (2019).

2. J. Liu, S. K. Lau, V. A. Varma, R. A. Moffitt, M. Caldwell, T. Liu, A. N. Young, J. A. Petros, A. O. Osunkoya, T. Krogstad, B. Leyland-Jones, M. D. Wang, S. Nie, Molecular mapping of tumor heterogeneity on clinical tissue specimens with multiplexed quantum dots. *ACS Nano* **4**, 2755–2765 (2010).

3. Q. Liu, J. Cai, Y. Zheng, Y. Tan, Y. Wang, Z. Zhang, C. Zheng, Y. Zhao, C. Liu, Y. An, C. Jiang, L. Shi, C. Kang, Y. Liu, NanoRNP overcomes tumor heterogeneity in cancer treatment. *Nano Lett.* **19**, 7662–7672 (2019).

4. D. Ling, W. Park, S.-j. Park, Y. Lu, K. Kim, M. J. Hackett, B. Kim, H. Yim, Y. Jeon, K. Na, T. Hyeon, Multifunctional tumor pH-sensitive self-assembled nanoparticles for bimodal imaging and treatment of resistant heterogeneous tumors. *J. Am. Chem. Soc.* **136**, 5647–5655 (2014).

5. A. Sharma, M.-G. Lee, M. Won, S. Koo, J. F. Arambula, J. L. Sessler, S.-G. Chi, J. S. Kim, Targeting heterogeneous tumors using a multifunctional molecular prodrug. *J. Am. Chem. Soc.* **141**, 15611–15618 (2019).

6. K. Melgar, M. M. Walker, L. M. Jones, L. C. Bolanos, K. Hueneman, M. Wunderlich, J.-K. Jiang, K. M. Wilson, X. Zhang, P. Sutter, A. Wang, X. Xu, K. Choi, G. Tawa, D. Lorimer, J. Abendroth, E. O'Brien, S. B. Hoyt, E. Berman, C. A. Famulare, J. C. Mulloy, R. L. Levine, J. P. Perentesis, C. J. Thomas, D. T. Starczynowskil, Overcoming adaptive therapy resistance in AML by targeting immune response pathways. *Sci. Transl. Med.* **11**, eaaw8828 (2019).

7. W. Fan, B. Yung, P. Huang, X. Chen, Nanotechnology for multimodal synergistic cancer therapy. *Chem. Rev.* **117**, 13566–13638 (2017).

8. Y. Ma, Y. Zhang, X. Li, Y. Zhao, M. Li, W. Jiang, X. Tang, J. Dou, L. Lu, F. Wang, Y. Wang, Near-infrared II phototherapy induces deep tissue immunogenic cell death and potentiates cancer immunotherapy. *ACS Nano*, **13**, 11967–11980 (2019).

9. L. Wu, D. Leng, D. Cun, C. Foged, M.Yang, Advances in combination therapy of lung cancer: Rationales, delivery technologies and dosage regimens. *J. Control. Release* **260**, 78–91 (2017).

10. R. van der Meel, E. Sulheim, Y. Shi, F. Kiessling, W. J. M. Mulder, T. Lammers. Smart cancer nanomedicine. *Nat. Nanotechnol.* **14**, 1007–1017 (2019).

11. Y. Cao, J. Arbiser, R. J. D'Amato, P. A. D'Amore, D. E. Ingber, R. Kerbel, M. Klagsbrun, S. Lim, M. A. Moses, B. Zetter, H. Dvorak, R. Langer, Forty-year journey of angiogenesis translational research. *Sci. Transl. Med.* **3**, 114rv3 (2011).

12. O. Takahashi, R. Komaki, P. D. Smith, J. M. Jürgensmeier, A. Ryan, B. N. Bekele, I. I. Wistuba, J. J. Jacoby, M. V. Korshunova, A. Biernacka, B. Erez, K. Hosho, R. S. Herbst, M. S. O'Reilly, Combined MEK and VEGFR inhibition in orthotopic human lung cancer models results in enhanced inhibition of tumor angiogenesis, growth, and metastasis. *Clin. Cancer Res.* **18**, 1641–1654 (2012).

13. J. M. L. Ebos, C. R. Lee, W. Cruz-Munoz, G. A. Bjarnason, J. G. Christensen, R. S. Kerbell, Accelerated metastasis after short-term treatment with a potent inhibitor of tumor angiogenesis. *Cancer Cell* **15**, 232–239 (2009).

14. M. Pàez-Ribes, E. Allen, J. Hudock, T. Takeda, H. Okuyama, F. Viñals, M. Inoue, G. Bergers, D. Hanahan, O. Casanovas, Antiangiogenic therapy elicits malignant progression of tumors to increased local invasion and distant metastasis. *Cancer Cell* **15**, 220–231 (2009).

15. L. Tian, A. Goldstein, H. Wang, H. C. Lo, I. S. Kim, T. Welte, K. Sheng, L. E. Dobrolecki, X. Zhang, N. Putluri, T. L. Phung, S. A. Mani, F. Stossi, A. Sreekumar, M. A. Mancini, W. K. Decker, C. Zong, M. T. Lewis, X. H.-F. Zhang, Mutual regulation of tumour vessel normalization and immunostimulatory reprogramming. *Nature* **544**, 250–254 (2017)

16. S. Huang, K. Shao, Y. Liu, Y. Kuang, J. Li, S. An, Y. Guo, H. Ma, C. Jiang, Tumor-targeting and microenvironment-responsive smart nanoparticles for combination therapy of antiangiogenesis and apoptosis. *ACS Nano* **7**, 2860–71 (2013).

17. L. Z. Gao, J. Zhuang, L. Nie, J. Zhang, Y. Zhang, N. Gu, T. Wang, J. Feng, D. Yang, S. Perrett, X. Yan, Intrinsic peroxidase-like activity of ferromagnetic nanoparticles. *Nat. Nanotechnol.* **2**, 577–583 (2007).

18. H. Wei, E. K. Wang, Nanomaterials with enzyme-like characteristics (nanozymes): Next-generation artificial enzymes. *Chem. Soc. Rev.* **42**, 6060–6093 (2013).

19. Y. Lin, J. Ren, X. Qu, Nano-gold as artificial enzymes: Hidden talents. *Adv. Mater.* **26**, 4200–4217 (2014).

20. L. Z. Gao, X. Y. Yan, Nanozymes: An emerging field bridging nanotechnology and biology. *Sci. China Life Sci.* **59**, 400–402 (2016).

21. X. Y. Wang, Y. H. Hu, H. Wei, Nanozymes in bionanotechnology: From sensing to therapeutics and beyond. *Inorg. Chem. Front.* **3**, 41–60 (2016).

22. W. He, W. Warner, Q. Xia, J.-j. Yin, P. P. Fu, Enzyme-like activity of nanomaterials. *J. Environ. Sci. Health C* **32**, 186–211 (2014).

23. Z. Tang, Y. Liu, M. He, W. Bu, Chemodynamic therapy: Tumour microenvironment-mediated Fenton and Fenton-like reactions. *Angew. Chem. Int. Ed.* **58**, 946–956 (2019).

24. K. Fan, J. Xi, L. Fan, P. Wang, C. Zhu, Y. Tang, X. Xu, M. Liang, B. Jiang, X. Yan, L. Gao, In vivo guiding nitrogen-doped carbon nanozyme for tumor catalytic therapy. *Nat. Commun.* **9**,1440 (2018).

25. Y. Du, B. Xu, T. Fu, M. Cai, F. Li, Y. Zhang, Q. Wang, Near-infrared photoluminescent Ag_2S quantum dots from a single source precursor. *J. Am. Chem. Soc.* **132**, 1470–1471 (2010).

26. Z. Yang, T. Zhao, X. Huang, X. Chu, T. Tang, Y. Ju, Q. Wang, Y. Hou, S. Gao, Modulating the phases of iron carbide nanoparticles: From a perspective of interfering with the carbon penetration of $Fe@Fe_3O_4$ by selectively adsorbed halide ions. *Chem. Sci.* **8**, 473–481 (2017).

27. Y. Ju, H. Zhang, J. Yu, S. Tong, N. Tian, Z. Wang, X. Wang, X. Su, X. Chu, J. Lin, Y. Ding, G. Li, F. Sheng, Y. Hou, Monodisperse Au–Fe_2C Janus nanoparticles: An attractive multifunctional

material for triple-modal imaging-guided tumor photothermal therapy. *ACS Nano* **11**, 9239–9248 (2017).

28. L. Chen, S. Yu, H. Wang, J. Xu, C. Liu, W. H. Chong, H. Chen, General methodology of using oil-in-water and water-in-oil emulsions for coiling nanofilaments. *J. Am. Chem. Soc.* **135**, 835–843 (2013).

29. Y.-P. Sun, B. Zhou, Y. Lin, W. Wang, K. A. S. Fernando, P. Pathak, M. J. Meziani, B. A. Harruff, X. Wang, H. Wang, P. G. Luo, H. Yang, M. E. Kose, B. Chen, L. M. Veca, S.-Y. Xie, Quantum-sized carbon dots for bright and colorful photoluminescence. *J. Am. Chem. Soc.* **128**, 7756–7757 (2006).

30. K. Avgoustakis, A. Beletsi, Z. Panagi, P. Klepetsanis, A. G. Karydas, D. S. Ithakissios, PLGA–mPEG nanoparticles of cisplatin: In vitro nanoparticle degradation, in vitro drug release and in vivo drug residence in blood properties. *J. Control. Release* **79**, 123–135 (2002).

31. M. Semeniuk, Z. Yi, V. Poursorkhabi, J. Tjong, S. Jaffer, Z.-H. Lu, M. Sain, Future perspectives and review on organic carbon dots in electronic applications. *ACS Nano* **13**, 6224–6255 (2019).

32. R.F. Egerton, M.J. Whelan, Electron energy loss spectra of diamond, graphite and amorphous carbon. *J. Electron. Spectros. Relat. Phenomena* **3**, 232–236 (1974).

33. Y. Zhong, Z. Ma, F. Wang, X. Wang, Y. Yang, Y. Liu, X. Zhao, J. Li, H. Du, M. Zhang, Q. Cui, S. Zhu, Q. Sun, H. Wan, Y. Tian, Q. Liu, W. Wang, K. C. Garcia, H. Dai, In vivo molecular imaging for immunotherapy using ultra-bright near-infrared-IIb rare-earth nanoparticles. *Nat. Biotechnol.* **37**, 1322–1331 (2019).

34. B. Du, M. Yu, J. Zheng, Transport and interactions of nanoparticles in the kidneys. *Nat. Rev. Mater.* **3**, 358–374 (2018)

35. J. Kim, H. R. Cho, H. Jeon, D. Kim, C. Song, N. Lee, S. H. Choi, T. Hyeon, Continuous O_2-evolving $MnFe_2O_4$ nanoparticle-anchored mesoporous silica nanoparticles for efficient photodynamic therapy in hypoxic cancer. *J. Am. Chem. Soc.* **139**, 10992–10995 (2017).

36. Z. Wang, Y. Ju, S. Tong, H. Zhang, J. Lin, B. Wang, Y. Hou, Au_3Cu tetrapod nanocrystals: Highly efficient and metabolizable multimodality imaging-guided NIR-II photothermal agents. *Nanoscale Horiz.* **3**, 624–631 (2018).

37. Z. Wang, Y. Ju, Z. Ali, H. Yin, F. Sheng, J. Lin, B. Wang, Y. Hou, Near-infrared light and tumor microenvironment dual responsive size-switchable nanocapsules for multimodal tumor theranostics. *Nat. Commun.* **10**, 4418 (2019)

38. Y. Yang, Q. Chen, S. Li, W. Ma, G. Yao, F. Ren, Z. Cai, P. Zhao, G. Liao, J. Xiong, Z. Yu, iRGD-mediated and enzyme-induced precise targeting and retention of gold nanoparticles for the enhanced imaging and treatment of breast cancer. *J. Biomed. Nanotechnol.* **14**, 1396–1408 (2018).

39. Y. Zhang, G. Hong, Y. Zhang, G. Chen, F. Li, H. Dai, Q. Wang. Ag_2S quantum dot: A bright and biocompatible fluorescent nanoprobe in the second near-infrared window. *ACS Nano* **6**, 3695–3702 (2012).